Cell Reports

Report

Huntingtin Aggregation Impairs Autophagy, Leading to Argonaute-2 Accumulation and Global MicroRNA Dysregulation

Graphical Abstract

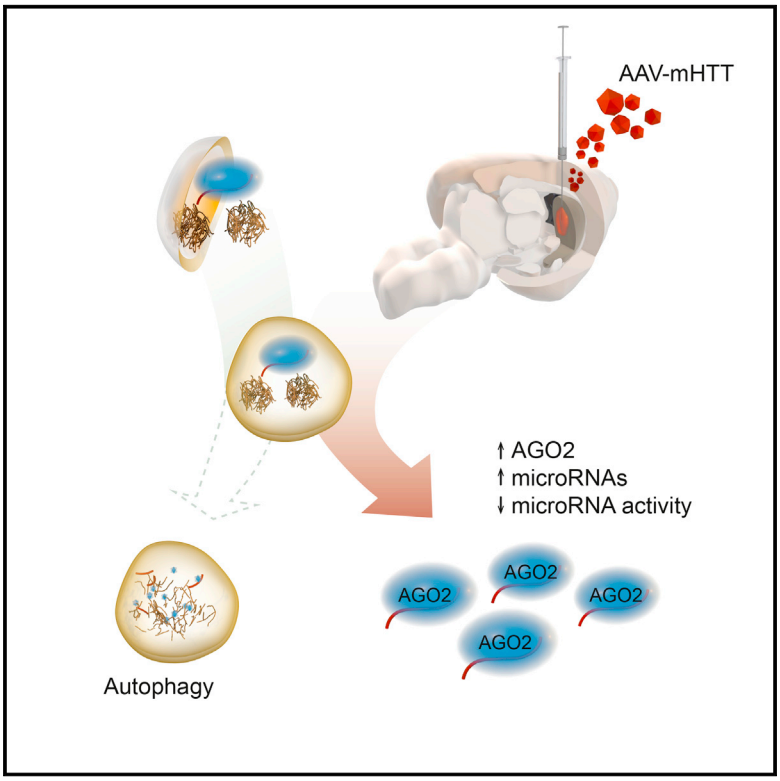

Authors

Karolina Pircs, Rebecca Petri, Sofia Madsen, ..., Malin Parmar, Roger A. Barker, Johan Jakobsson

Correspondence

johan.jakobsson@med.lu.se

In Brief

Pircs et al. report that aggregation of the mutant huntingtin protein, a hallmark of Huntington's disease proteinopathy, impairs macroautophagy, leading to Argonaute-2 accumulation and global dysregulation of microRNAs. These results indicate that autophagy not only influences protein aggregation but also directly contributes to the global alterations of post-transcriptional networks in Huntington's disease.

Highlights

- Mutant HTT overexpression causes impairment of autophagy, resulting in AGO2 accumulation
- Activation of autophagy reverses AGO2 accumulation in neurons
- AGO2 accumulation results in a global increase in miRNA levels
- AGO2 re-localizes to stress granules, resulting in loss of miRNA activity

Data and Software Availability

GSE78928

Pircs et al., 2018, Cell Reports *24*, 1397–1406
August 7, 2018
https://doi.org/10.1016/j.celrep.2018.07.017

CellPress

Cell Reports
Report

Huntingtin Aggregation Impairs Autophagy, Leading to Argonaute-2 Accumulation and Global MicroRNA Dysregulation

Karolina Pircs,[1] Rebecca Petri,[1] Sofia Madsen,[1] Per Ludvik Brattås,[1] Romina Vuono,[2] Daniella R. Ottosson,[3] Isabelle St-Amour,[4] Bob A. Hersbach,[1] Monika Matusiak-Brückner,[1] Sofia Hult Lundh,[5] Åsa Petersén,[5] Nicole Déglon,[6] Sébastien S. Hébert,[4] Malin Parmar,[3] Roger A. Barker,[2,3] and Johan Jakobsson[1,7,*]

[1]Laboratory of Molecular Neurogenetics, Department of Experimental Medical Science, Wallenberg Neuroscience Center and Lund Stem Cell Center, BMC A11, Lund University, 221 84 Lund, Sweden

[2]John van Geest Centre for Brain Repair and Department of Neurology, Department of Clinical Neurosciences, University of Cambridge, Forvie Site, Cambridge CB2 0PY, UK

[3]Developmental and Regenerative Neurobiology, Department of Experimental Medical Science, Wallenberg Neuroscience Center and Lund Stem Cell Center, BMC A11, Lund University, 221 84 Lund, Sweden

[4]Axe Neurosciences, Centre de Recherche du CHU de Québec – Université Laval, CHUL, Québec, QC G1V 4G2, Canada

[5]Translational Neuroendocrine Research Unit (TNU), Department of Experimental Medical Science, Wallenberg Neuroscience Center, BMC D11, Lund University, 221 84 Lund, Sweden

[6]Laboratory of Cellular and Molecular Neurotherapies (LCMN), Department of Clinical Neuroscience (DNC), Neuroscience Research Center (CRN), Lausanne University Hospital (CHUV), 1011 Lausanne, Switzerland

[7]Lead Contact

*Correspondence: johan.jakobsson@med.lu.se

https://doi.org/10.1016/j.celrep.2018.07.017

SUMMARY

Many neurodegenerative diseases are characterized by the presence of intracellular protein aggregates, resulting in alterations in autophagy. However, the consequences of impaired autophagy for neuronal function remain poorly understood. In this study, we used cell culture and mouse models of huntingtin protein aggregation as well as post-mortem material from patients with Huntington's disease to demonstrate that Argonaute-2 (AGO2) accumulates in the presence of neuronal protein aggregates and that this is due to impaired autophagy. Accumulation of AGO2, a key factor of the RNA-induced silencing complex that executes microRNA functions, results in global alterations of microRNA levels and activity. Together, these results demonstrate that impaired autophagy found in neurodegenerative diseases not only influences protein aggregation but also directly contributes to global alterations of intracellular post-transcriptional networks.

INTRODUCTION

MicroRNAs (miRNAs) are small non-coding RNAs that provide post-transcriptional control of gene expression. miRNAs play an important role in the brain, where hundreds of different miRNAs are expressed and thought to regulate thousands of transcripts (Petri et al., 2014). Several lines of evidence indicate that miRNAs are likely to play an important role in neurodegenerative diseases (NDDs) (Maciotta et al., 2013). For example, conditional deletion of *Dicer*, a key enzyme in the miRNA biogenesis pathway, results in neuronal cell death (Pang et al., 2014). In addition, there are numerous reports describing changes in miRNA expression levels in NDDs such as Alzheimer's disease (AD), Parkinson's disease (PD), Huntington's disease (HD), and amyotrophic lateral sclerosis (ALS) (Maciotta et al., 2013). It is therefore likely that alterations in miRNA levels participate in the pathophysiological events underlying cell dysfunction and loss in these diseases.

AD, PD, HD, ALS, and other diseases form a large class of NDDs known as proteinopathies, characterized by the formation of specific protein aggregates in the brain. Neurons appear to be particularly sensitive to aggregation-prone proteins, indicating that neuronal survival is highly dependent on maintaining efficient protein quality control with rapid removal of toxic and aggregated proteins (Cortes and La Spada, 2014). However, it remains unclear how protein aggregation influences intracellular functions and why specific neuronal subtypes ultimately are lost in these different disorders. For example, it is well established that neuronal gene expression programs are severely altered in these disorders, but mechanistic insight into how neuronal protein aggregation results in selective disturbances in transcriptional networks is currently lacking.

Macroautophagy (hereafter referred to as autophagy) is an evolutionary conserved lysosomal degradation pathway characterized by the formation of an autophagosome, a double-membraned vesicle that isolates the cytoplasmic cargo for destruction (Martin et al., 2015). The autophagosome ultimately fuses with a lysosome, forming the autolysosome where the cargo is degraded. Several studies have documented altered autophagy in NDDs, and boosting autophagy has been proposed as a novel therapeutic strategy (Martin et al., 2015). In addition to clearing toxic and misfolded

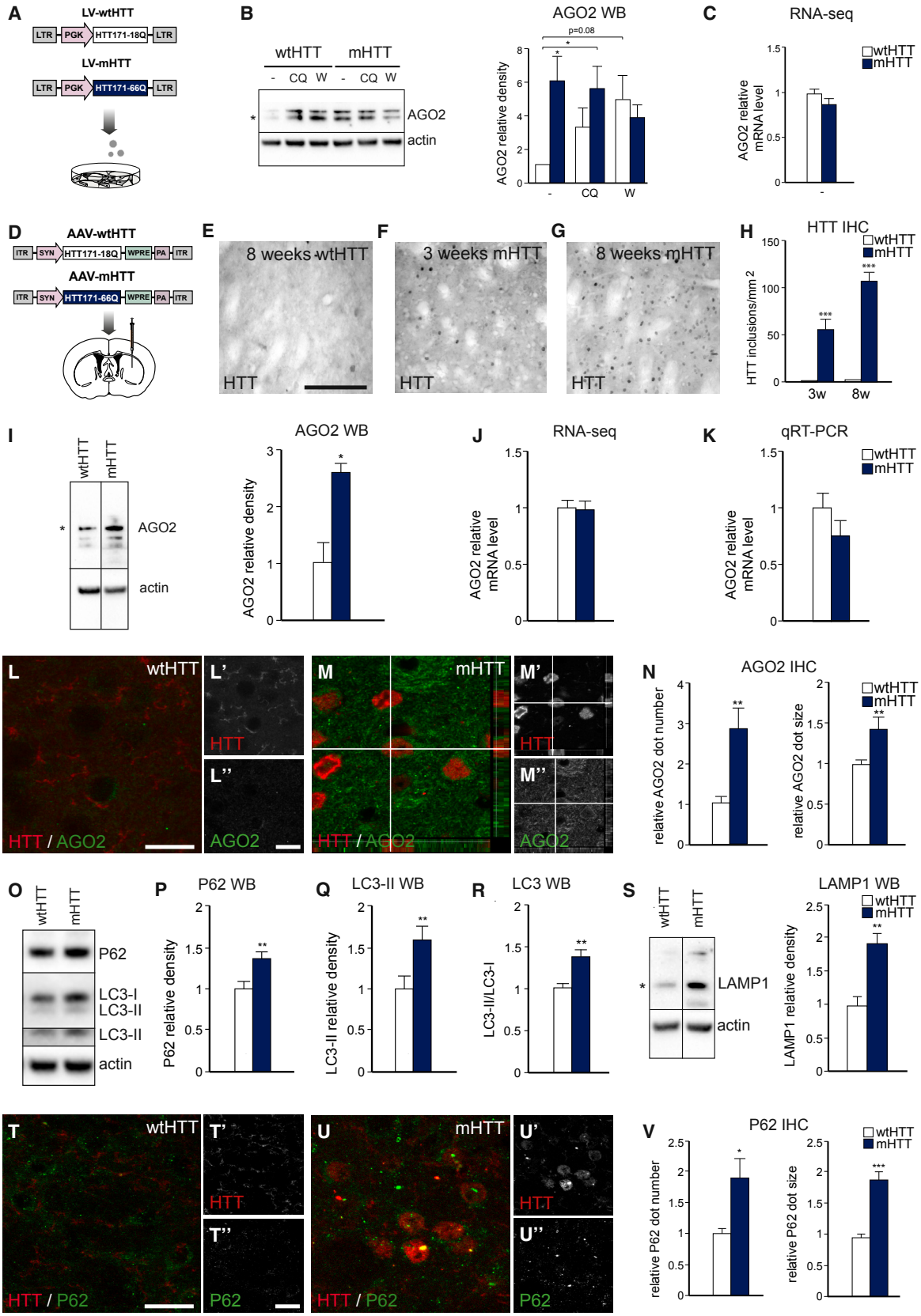

(legend on next page)

proteins, we and others have recently found that autophagy also plays a critical role in maintaining brain homeostasis through selective protein degradation (Petri et al., 2017; Yamamoto and Yue, 2014). One possibility is therefore that alterations of autophagy in NDDs also directly influence other intracellular neuronal functions.

One protein that is of interest in this regard is Argonaute-2 (AGO2), which is degraded by selective autophagy under basal conditions (Gibbings et al., 2012). AGO2 is a core component of the RNA-induced silencing complex (RISC), which executes miRNA functions. In the RISC, AGO2 has multiple roles, including biogenesis and maturation of miRNAs, as well as direct binding of mature miRNAs (Petri et al., 2014). AGO2 also provides endoribonuclease activity that enables direct degradation of miRNA target transcripts, as well as recruitment of other downstream factors that mediate transcriptional repression or decay (Bossé and Simard, 2010). Several studies have shown that intracellular AGO2 protein is carefully titrated at a post-transcriptional level and that miRNA-free AGO2 is degraded through a specific mechanism (Füllgrabe et al., 2014). Removal of mature miRNAs by deleting the miRNA biogenesis factors *Dgcr8* or *Dicer* results in a parallel reduction of AGO2 protein levels (Gibbings et al., 2012; Savas et al., 2008). Furthermore, overexpression of AGO2 is very difficult to achieve, further suggesting a feedback regulation of AGO2 protein levels (Füllgrabe et al., 2014; He et al., 2012). Together, these observations indicate that the regulation of intracellular AGO2 protein levels is critical in maintaining appropriate miRNA activity.

In this study, we used both cell culture and mouse models as well as post-mortem material from patients with HD to demonstrate that AGO2 accumulates as a result of impaired autophagy in neurons expressing aggregating mutant Huntingtin (mHTT). This AGO2 accumulation results in a global alteration of miRNA activity. Our results provide mechanistic insights into how impairment in autophagy in NDDs contributes to dysregulation of miRNA networks.

RESULTS

mHTT-Mediated Impairment of Autophagy Correlates with Accumulation of AGO2

To investigate a potential link between alterations in autophagy in NDDs and AGO2 expression levels, we transduced 293T cells with lentiviral vectors expressing exon 1 of wild-type *HTT* (*wtHTT*, 18 polyQ repeats) or mutant *HTT* (*mHTT* 66Q, 66 polyQ repeats) (Figure 1A). *HTT* is mutated in HD, where a polyglutamine expansion in the first exon ultimately leads to a toxic gain of function for *mHTT* and protein aggregation (DiFiglia et al., 1997). Vector transduction was also combined with chloroquine (CQ) treatment, which prevents both the fusion of the autophagosome with the lysosome and lysosomal protein degradation, or with wortmannin (W) treatment, a phosphatidylinositol 3-kinase (PI3K) inhibitor that provides an early block of autophagy and inhibits microtubule-associated protein 1A/1B-light chain 3 (LC3) lipidation. Using this system, we monitored autophagic activity by assessing the levels of LC3II, LC3-II/ I ratio, p62, and LAMP1 using western blot (WB) and immunocytochemistry (ICC) and found, in line with other studies (Martin et al., 2015), that expression of mHTT mediates a late-step block of autophagy characterized by failure of fusion of the autophagosome and the lysosome (Figures S1A–S1R).

We next investigated AGO2 expression levels using WB in 293T cells transduced with mHTT. We found a significant increase in the AGO2 protein level compared to wtHTT-expressing cells, whereas there was no difference in the AGO2 mRNA level (Figures 1B, 1C, and S1S). A similar increase in AGO2 protein was also seen in wtHTT-transduced cells when we inhibited autophagy using CQ or W (Figures 1B, 1C, and S1S), whereas we found no additive effect of mHTT expression after CQ or W treatment. Together, these data demonstrate that mHTT-mediated autophagy impairment results in accumulation of AGO2 at a post-transcriptional stage in mHTT-expressing cells in a manner similar to that seen following chemical autophagy inhibition.

Figure 1. mHTT Expression Alters Autophagy and Results in Accumulation of AGO2 *In Vitro* and *In Vivo*

(A) Diagrams of the lentivrus (LV)-*mHTT* and LV-*wtHTT* vectors and the experimental workflow, showing transduction of 239T cells before assays.

(B) There was an elevated expression of AGO2 protein in mHTT-expressing cells. AGO2 protein levels increased after autophagic impairment induced by CQ or W in LV-wtHTT-overexpressing cells. AGO2 protein is marked with an asterisk. n = 5.

(C) There was no change in the mRNA level of the AGO2 protein in LV-mHTT- or LV-wtHTT-expressing 293T cells. n = 3.

(D) Diagrams of the AAV-*mHTT* and AAV-*wtHTT* vectors and the experimental workflow.

(E–H) Time-dependent accumulation of HTT was present in AAV-*mHTT* injected animals after 3 (F) and 8 (G) weeks, but not in AAV-*wtHTT* (E)-injected animals. (H) Number of HTT aggregates/ mm^2. n = 45 (3 animals/ group).

(I) AGO2 protein accumulates after 3 weeks in AAV-*mHTT*-injected animals. AGO2 protein is marked with an asterisk. n = 8 (4 animals/ group).

(J) AGO2 mRNA levels were not changed 3 weeks after mHTT overexpression. n = 3.

(K) Relative AGO2 mRNA levels were not changed 3 weeks after mHTT overexpression. n = 5.

(L–N) AGO2 protein accumulates in AAV-*mHTT* (M), but not in AAV-*wtHTT* (L)-injected animals 8 weeks after injection. (N) There were significantly more, as well as bigger puncta in the AAV-*mHTT*-injected mice than in those injected with AAV-*wtHTT*. n = 27 (3 animals/ group).

(O–R) WB autophagic protein expression levels in AAV-*mHTT* and *wtHTT*-injected animals (O). Increased expression levels of the autophagic markers p62 (P) and LC3-II (Q) and LC3-II/LC3-I ratio (R) are detected 3 weeks after AAV-*mHTT* injections. n = 8 (4 animals/ group).

(S) Accumulation of LAMP1 was seen after 3 weeks in AAV-*mHTT*-injected but not in AAV-*wtHTT*-injected mice. LAMP1 is marked with an asterisk. n = 10 and 20 for wtHTT and mHTT, respectively (4 animals/ group).

(T–V) IHC demonstrate p62 accumulation in the AAV-*mHTT* (U) compared to AAV-*wtHTT* (T)-injected animals. (V) Relative p62 dot number and size were significantly increased in mHTT-overexpressing animals compared to wtHTT 8 weeks after injection. n = 19 and 24 for AAV-*wtHTT*- and AAV-*mHTT*-injected animals, respectively (3 animals/ group).

WB values were normalized to LV-wtHTT non-treated (B) or AAV-wtHTT (I and O–S) expression levels and corrected to actin values. ***$p < 0.001$, **$p < 0.01$, *$p < 0.05$; nonparametric Kruskal-Wallis test was used for (B); two-tailed two-sample unequal variance t tests were used for all other cases. All data are shown as mean ± SEM. Scale bars represent 50 μm (E–G), 10 μm (L and M), and 10 μm (T and U). See also Figures S1–S3 and S6 and Tables S1 and S3.

AGO2 Accumulates in Striatal Neurons Expressing mHTT

The most affected neuronal cell type in HD is medium spiny neurons in the striatum. To study the role of mHTT in modulating autophagy and AGO2 levels in striatal neurons *in vivo*, we generated adeno-associated viral (AAV) vectors expressing either exon 1 *wtHTT* or *mHTT* under the control of the neuron-specific synapsin promoter that were subsequently injected into the striatum of the mouse brain (Figure 1D). Mice injected with AAV-*mHTT* showed a progressive increase in intracellular mHTT inclusions, whereas AAV-*wtHTT* did not develop such inclusions (Figures 1E–1H). We also found progressive loss of DARPP-32 levels in AAV-*mHTT*-injected mice in the absence of neuronal cell loss, indicating progressive dysfunction of striatal medium spiny neurons (Figures S2A–S2E).

We next investigated AGO2 levels after AAV-*mHTT* injections using WB and found an almost 3-fold increase 3 weeks post-injection (Figure 1I). We did not observe any changes in AGO2 mRNA levels, as monitored by RNA sequencing (RNA-seq) or by qRT-PCR (Figures 1J and 1K). When we investigated AGO2 expression in the striatum using immunohistochemistry (IHC) with two different antibodies, we found cytoplasmic AGO2 protein accumulation in the animals injected with AAV-*mHTT* but not in animals injected with AAV-*wtHTT* (Figures 1L–1N and S3A–S3D). We did not see any colocalization between AGO2 and mHTT aggregates in animals injected with AAV-*mHTT*, suggesting that AGO2 accumulation is not a result of direct binding to HTT aggregates (Figures 1L–1N). We also investigated the level of other AGO proteins in the presence of mHTT but did not find any changes in the protein or mRNA level for AGO1 and AGO4 (Figures S3E–S3G). Together, these data show that expression of mHTT in striatal neurons results in protein aggregation that is associated with formation and accumulation of AGO2 protein puncta.

Activation of Autophagy Reverses AGO2 Accumulation in Striatal Neurons Expressing mHTT

We next investigated alterations in autophagy following AAV-*mHTT* injections in the mouse brain. Using WB and IHC analysis of dissected striatal tissue from mice injected with AAV-*mHTT* and AAV-*wtHTT*, we found increased levels of p62 and LC3-II as well as an increased LC3-II/I ratio, suggesting impaired autophagosome-lysosome fusion or inhibition of lysosome-mediated proteolysis (Figures 1O–1R, S3H, and S3I). We also found an increase in the lysosomal marker LAMP1 (Figures 1S, S3J, and S3K). We found no changes in the mRNA levels of any of these markers, as monitored by RNA-seq (Figures S3L–S3N). Confocal analysis of HTT/p62 co-staining revealed numerous p62-positive mHTT aggregates in AAV-*mHTT* animals (Figures 1T–1V). p62-positive clusters were found to accumulate adjacent to the protein aggregates, with significant p62 sequestration within aggregates (Figure S3O). Although accumulated p62 and AGO2 puncta were often found in the same cells, we never saw colocalization of these two proteins, which is in line with previous data showing that AGO2 is degraded by autophagy in a p62-independent manner (Figures S3P–S3S; Table S1; Gibbings et al., 2012; Savas et al., 2008). In addition, AGO2 puncta never colocalized with the autophagosomal marker LC3 in mHTT-expressing cells, whereas we found several examples of colocalization between AGO2 and LC3 in wtHTT-expressing neurons, indicating that AGO2 is selectively degraded by autophagy in neurons expressing the wt protein but not in neurons expressing the mutant protein (Figures S3T and S3U). Together, these results demonstrate that expression of mHTT leads to a distinct impairment in autophagy that correlates with the accumulation of AGO2.

To provide a mechanistic link between the decrease in autophagy activity and AGO2 accumulation, we next overexpressed Beclin-1 (BECN1), a positive regulator of autophagosome formation, together with mHTT in the mouse brain (Figures S4A and S4B). Three weeks after co-delivery of AAV-*mHTT* and AAV-*BECN1*, the number of p62 aggregates was dramatically lower compared to animals injected with AAV-*mHTT* alone (Figures 2A–2C). We also measured the changes in the level of LC3 with WB and IHC to see whether there was increased autophagy activity and found a significant increase in the level of LC3-II and LC3-II/I ratio (Figure S4C). LC3-positive dots accumulated in the co-injected animals around the mHTT aggregates (Figures S4D and S4E). We did not detect any changes in the level of LAMP1 using IHC or WB, indicating that BECN1 overexpression did not affect the formation and amount of lysosomes or endosomes (Figures S4F–S4I). We also found that BECN1 accumulated around mHTT inclusions, which is in line with its association with newly formed autophagosomes (Figures S4J–S4L).

Strikingly, AGO2 dot number and size were significantly reduced in BECN1 co-expressing mice (Figures 2D–2F). Thus, BECN1 co-overexpression decreased the number of p62 aggregates and reduced AGO2 dot size and number, providing a mechanistic link between autophagy and AGO2 accumulation.

It is worth noting that the number of HTT inclusions was 3 times less in co-injected mice than in animals injected with AAV-*mHTT* only (Figures 2G–2I) and that the DARPP-32 levels in striatal projection neurons were significantly higher (Figure 2J), suggesting that autophagy activation using AAV-*BECN1* interferes with the progression of the mHTT-associated disease phenotype.

AGO2 Accumulation in a HD Mouse Model and Post-mortem HD Tissue

Although the AAV-*mHTT* model is a good tool to study protein aggregation in neurons, it fails to recapitulate many of the features of HD (e.g., pathology in non-neuronal cells). To investigate a potential dysregulation of AGO2 in a more disease-relevant model of HD, we used BACHD mice, which express full-length mHTT with 97 glutamine repeats under the control of endogenous HTT regulatory sequences (Gray et al., 2008). At 6 months of age, which represents an early manifest stage, we found an accumulation of p62 inclusions in striatal neurons of BACHD mice that was not seen in striatal tissue from wt littermates (Figures 3A–3D). We also detected AGO2 accumulation in striatal tissue of BACHD mice but not in controls (Figures 3A–3C and 3E). These AGO2 puncta were primarily found in the cytoplasm of cells with a neuronal morphology. As with the AAV-model, we never saw colocalization of p62 and AGO2 protein, although p62 aggregates and AGO2 puncta were often found in the same cells (Figure 3F; Table S1).

We then performed IHC on post-mortem striatal material from HD patients of different pathological grades and healthy

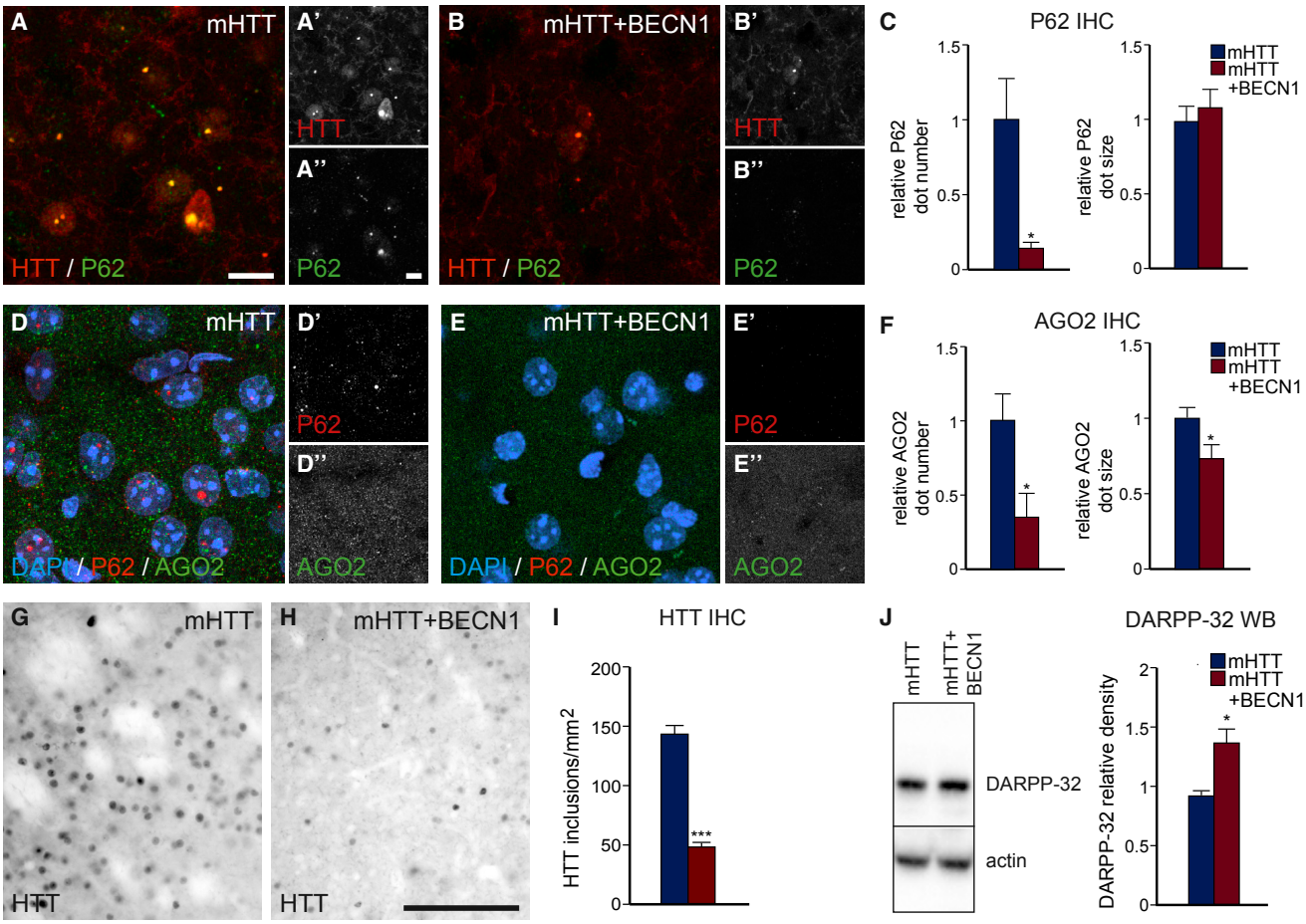

Figure 2. AAV-Mediated Delivery of Beclin1 Reverses mHTT-Associated Phenotypes

(A–C) Co-injection of AAV-*BECN1* and AAV-*mHTT* (B) reversed the aggregation of HTT and p62 compared to AAV-*mHTT* (A)-injected animals. (C) There was a reduction in the number, but not in the size of p62 aggregates. n = 10 (3 animals/group).

(D–F) IHC demonstrate decreased AGO2 accumulation in the co-injected animals (E) compared to the AAV-*mHTT* (D). (F) Overexpression of BECN1 and mHTT significantly decreased AGO2 accumulation in both number and size. n = 10 (3 animals/group).

(G–I) IHC demonstrate decreased HTT aggregation in the co-injected animals (H) compared to the AAV-*mHTT* (G). (I) Overexpression of BECN1 greatly reduced the number of HTT aggregates. n = 41 for AAV-*mHTT*, and n = 61 for AAV-*BECN1*+*mHTT* (3 animals/group).

(J) The DARPP-32 protein level was significantly higher in AAV-*BECN1*-co-injected animals compared to *mHTT*-injected animals. n = 10 (3 animals/group). WB values were normalized to AAV-*mHTT* injection expression levels and corrected to actin values. ***$p < 0.001$, *$p < 0.05$, two-tailed two-sample unequal variance t tests. All data are shown as mean ± SEM. Scale bars represent 37.5 μm (A, B, D, and E) and 50 μm (G and H). See also Figure S4.

age-matched individuals (Table S2). We found AGO2 accumulation in cells in striatal tissue of the HD patients but not in healthy individuals (Figure 3G–3M). We also found accumulation of p62 adjacent to mHTT inclusions in the neurons that were not seen in the striatal tissue of healthy individuals (Figures S5A and S5B). Similarly, we did not see colocalization of p62 and AGO2 protein (Figure 3N; Table S1). These data demonstrate that AGO2 accumulates in a HD mouse model as well as in HD patients.

AGO2 Accumulation Results in a Global Increase in miRNA Levels

AGO2 levels are directly related to the number of mature miRNAs present within a cell (Diederichs and Haber, 2007). This suggests that the increase in AGO2 levels that occurs following mHTT expression may result in an increased level of mature miRNAs, which may be coupled to profound effects on the activity of miRNAs. To investigate alterations in miRNA levels, we performed small RNA-seq on striatal brain tissue dissected 3 weeks after AAV-*wtHTT* and AAV-*mHTT* injections. This time point was chosen because there were no major cell death or phenotypic changes in the surrounding glia and only minor electrophysiological alterations in striatal neurons, representing an early time point in the disease course (Figures S2F–S2Q and S5C; Table S3). When investigating global miRNA levels, we found a more than 50% global increase in mature miRNA levels in AAV-*mHTT*-injected mice compared to AAV-*wtHTT*-injected mice (Figures 4A and 4B). We found that most individual miRNAs were overexpressed, including abundant neuronal miRNAs such as miR-128, miR-9, and let-7

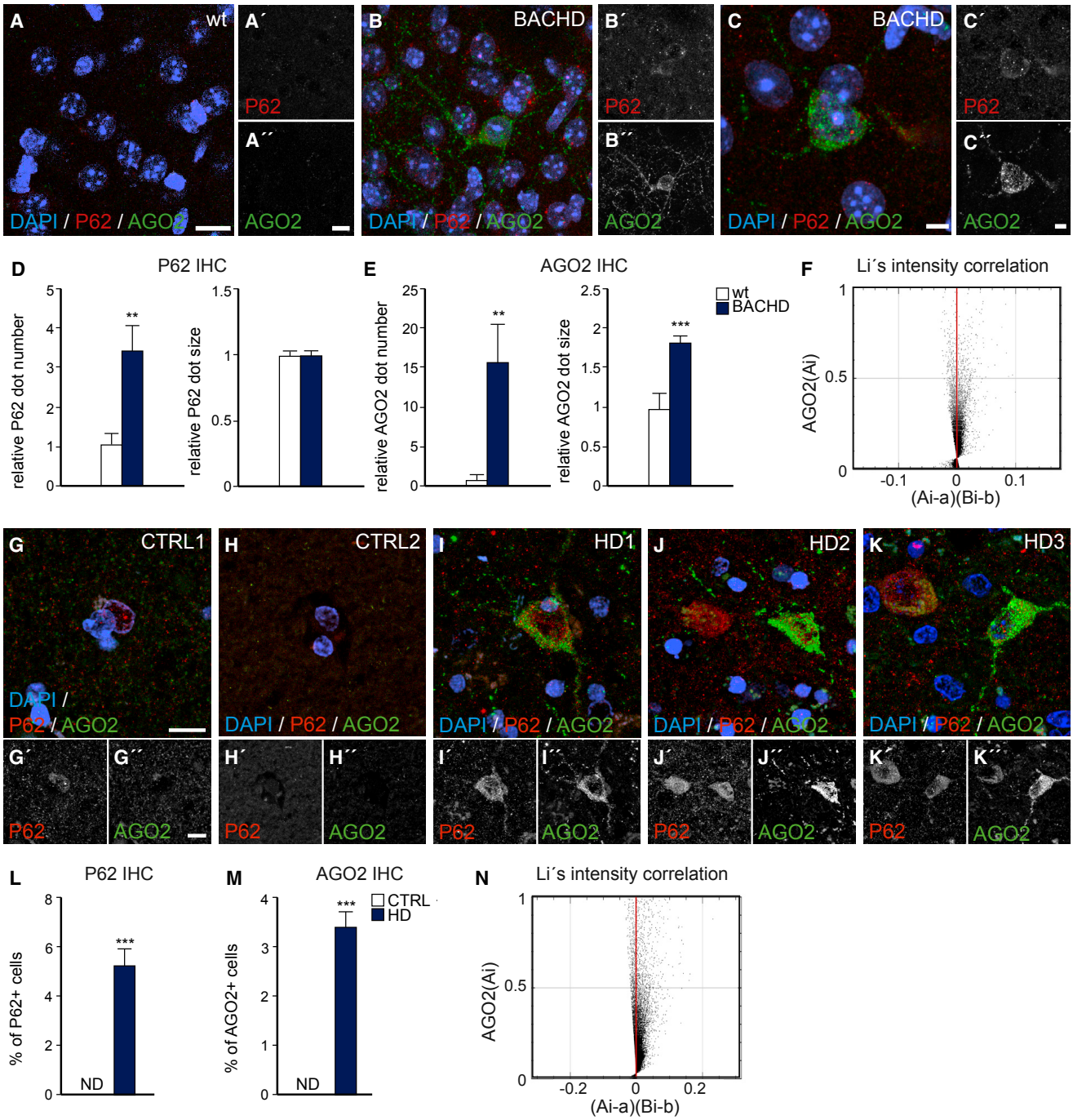

Figure 3. p62 and AGO2 Accumulate in BACHD Mice and in Post-mortem Material from HD Patients

(A–E) p62 (D) and AGO2 (E) accumulate in the striatal tissue of BACHD mice (B and C) but not in wt animals (A). n = 18 (3 animals/ group).

(F) Li's intensity correlation analysis shows that AGO2 and p62 have almost no colocalization, as indicated by the points mostly falling equally along the positive and negative sides of the x axis. Ai: AGO2 intensity; Bi: p62 intensity.

(G–M) There was a clear accumulation of AGO2 (M) and p62 (L) in all of the HD post-mortem tissue (I–K) but not in the healthy control tissue (G and H). (L) For p62 statistical analysis, 542 and 1,658 DAPI+ cells were analyzed in 2 control and 3 HD patients, respectively. (M) For AGO2 statistical analysis, 772 and 2,032 DAPI+ cells were analyzed in 2 control and 3 HD patients, respectively.

(N) AGO2 and p62 puncta accumulated inside neurons and did not colocalize. Ai: AGO2 intensity; Bi: p62 intensity.

ND: non-detectable; ***$p < 0.001$; **$p < 0.01$; two-tailed two-sample unequal variance t tests. All data are shown as mean ± SEM. Scale bars represent 25 μm (A and B), 5 μm (C), and 12.5 μm (G–K). See also Figure S5 and Tables S1 and S2.

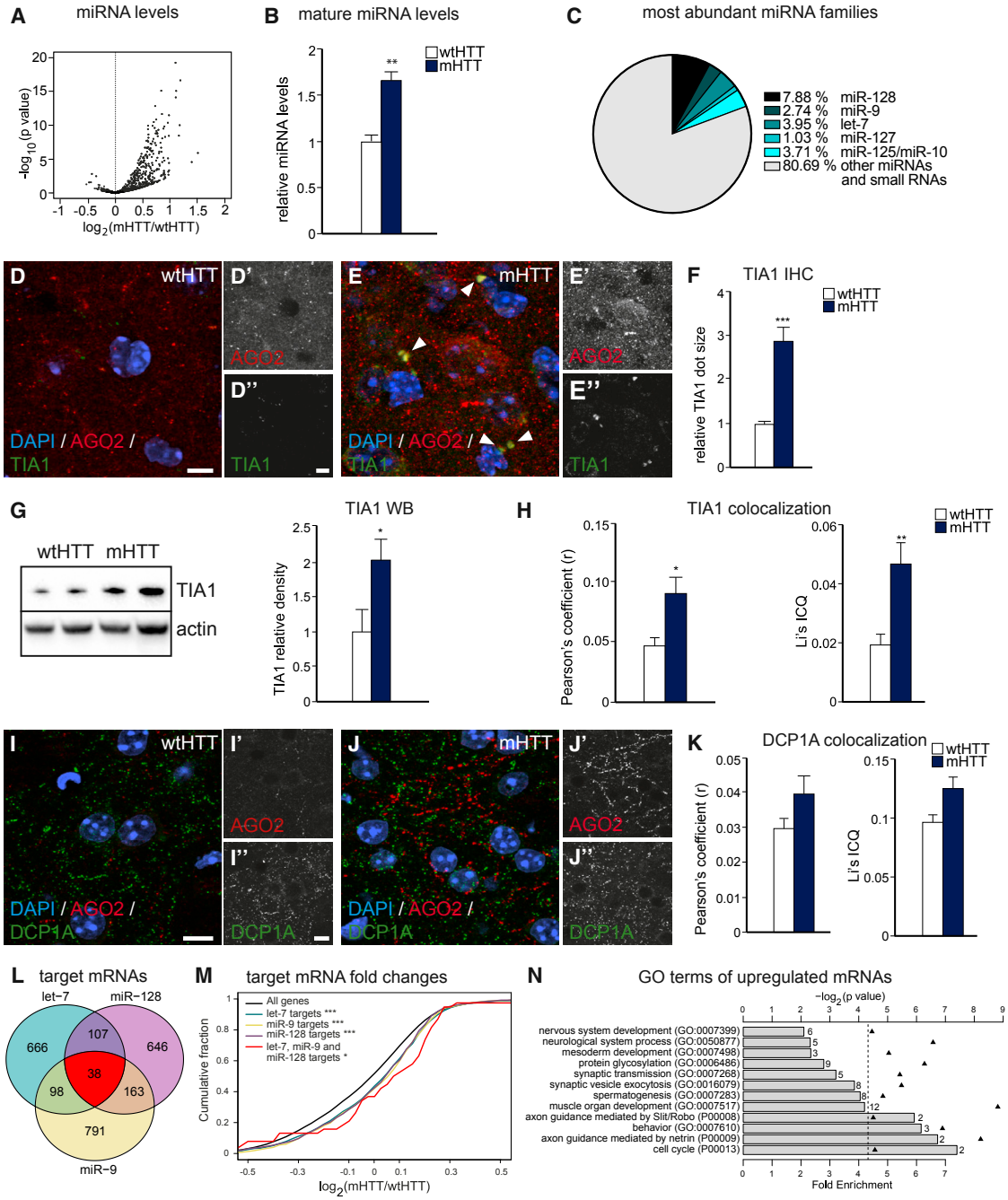

Figure 4. miRNAs and SGs Accumulate in Neurons Expressing Protein Aggregates

(A) Volcano plot summarizing the fold changes of all miRNAs after 3 weeks in AAV-*mHTT*-injected animals compared to AAV-*wtHTT*. n = 3 (8 animals/sample, Wald chi-square test).

(B) Levels of mature miRNAs are increased in AAV-*mHTT*-injected animals compared to AAV-*wtHTT*-injected controls 3 weeks after injection. n = 3 (8 animals/sample).

(C) Distribution of the most abundant miRNA families after 3 weeks of AAV-*wtHTT*-injected animals. n = 3 (8 animals/sample).

(D–F) TIA1 accumulated in AAV-*mHTT* (E)-injected animals compared to AAV-*wtHTT* (D). (F) Overexpression of mHTT significantly increased TIA1 size. n = 11 for AAV-*wtHTT* and n = 9 for AAV-*mHTT* (3 animals/group).

(G) TIA1 protein level was significantly higher in AAV-*mHTT*-injected animals compared to AAV-*wtHTT*. n = 10 or 8 (5 animals in the AAV-*wtHTT* group and 4 animals in the AAV-*mHTT*-injected group).

(H) TIA1 showed increased colocalization with AGO2. n = 11 for AAV-*wtHTT* and n = 9 for AAV-*mHTT* (3 animals/group).

(legend continued on next page)

(Figures 4C, S5D, and S5E). These data demonstrate that the increase in AGO2 levels correlates with an increased level of mature miRNAs.

AGO2 Puncta Localize to Stress Granules, Resulting in Loss of miRNA Activity

The subcellular localization of AGO2 is known to be important for the activity of miRNA-mediated gene silencing (Leung and Sharp, 2013). This suggests that alterations of AGO2 levels as well as accumulation of AGO2 in puncta in mHTT-expressing neurons may affect the activity of miRNAs. AGO2 protein is normally diffusely distributed throughout the cytoplasm but has also been found in processing bodies (P-bodies) and stress granules (SGs) (Anderson and Kedersha, 2006; Leung and Sharp, 2013). The shuffling of AGO2 through different cytoplasmic compartments is directly related to the activity of miRNAs. For example, AGO2 found in SGs contains miRNAs but does not participate in gene silencing (Leung and Sharp, 2013).

In mice injected with AAV-*mHTT*, we found a 4-fold increase in the size of SGs, as monitored with the cytotoxic granule-associated RNA binding protein TIA1 (Figures 4D–4F). We also found an increase in total TIA1 levels, as measured with WB (Figure 4G). Remarkably, we found a clear increase in the amount of AGO2 localizing to SGs in mHTT-expressing cells (Figures 4D, 4E, and 4H; Table S1). On the contrary, we did not find a significant increase in colocalization of AGO2 puncta to P-bodies (Figures 4I–4K; Table S1). We also found that overexpression of AAV-BECN1, together with AAV-mHTT, significantly reduced TIA1 colocalization with AGO2 (Figures S5F–S5H; Table S1). These data demonstrate that a substantial fraction of AGO2 re-localizes to SGs in mHTT-expressing neurons. Because AGO2-miRNA complexes lose their silencing activity in SGs, this indicates that an overall loss of miRNA activity should occur following mHTT expression.

To test this hypothesis, we investigated neuronal miRNA activity by performing RNA-seq on striatal tissue injected with either AAV-*mHTT* or AAV-*wtHTT* and quantified the expression of all detectable mRNAs. We then selected targets of three of the most highly expressed neuronal miRNAs in the mouse striatum, miR-128, let-7, and miR-9, based on computationally predicted and evolutionary conserved miRNA target sites (TargetScanMouse 7.1) (Figure 4L; Table S4; Agarwal et al., 2015). We assessed the global fold change distribution of targets in cumulative fraction graphs (y axis) and found that the expression levels of these miRNA targets, but not non-neuronal miRNA targets or non-targeted mRNAs, were significantly increased in AAV-*mHTT*-injected animals, indicating a de-repression of targets of the most abundant neuronal miRNAs (Figures 4M and S5I). Interestingly, genes targeted by all three miRNAs showed an even stronger shift toward de-repression (Figure 4M). Together, these results are in line with other studies where re-localization of AGO2 to SGs is associated with a loss of miRNA activity (Leung and Sharp, 2013; Qi et al., 2008; Wu et al., 2011).

To investigate the potential function of the de-repressed miRNA targets, we performed gene ontology analysis on the set of genes targeted by the three most abundant miRNAs (let-7, miR-128, and miR-9) and found these to be highly enriched for terms such as neurological system processes, axon guidance, and synaptic functions (Figures 4N and S5J). These are all mechanisms that are disrupted in HD and other NDDs. In an independent analysis, we also confirmed that experimentally identified neuronal miR-128 targets were upregulated upon mHTT expression (Figure S5K; Tan et al., 2013). It is worth noting that the phenotype of miR-128 KO mice is characterized by neuronal hyperactivity, a phenomenon that is also found in models of HD, directly linking our analysis to HD-like phenotypes (Tan et al., 2013).

DISCUSSION

Several hundred miRNAs are expressed in the brain and are thought to regulate thousands of transcripts (Petri et al., 2014). Therefore, any alteration in the miRNA network is likely to have a significant effect on neuronal function. In line with this, there is extensive literature documenting that conditional deletion of *Dicer* or individual miRNAs such as miR-128 in postmitotic neurons (including striatal neurons) results in phenotypes that are reminiscent of HD (Cheng et al., 2014; Schaefer et al., 2007; Tan et al., 2013). Thus, an alteration in miRNA activity in HD and other NDDs is likely to contribute to the early intracellular pathology, including alterations in neuronal activity and synaptic plasticity.

The current work provides mechanistic insight into how protein aggregation causes global alterations of miRNA level and activity through a direct link between impaired autophagy and AGO2 accumulation because of mHTT expression. Our results are in line with previous studies demonstrating that selective autophagy is required to maintain appropriate AGO2 levels and that AGO2 levels need to be carefully regulated to sustain appropriate levels of mature miRNAs (Füllgrabe et al., 2014; Gibbings et al., 2012; He et al., 2012; Savas et al., 2008). However, a previous study

(I–K) There was no difference in the level of AGO2 co-staining with DCP1A between AAV-*wtHTT* (I) and *mHTT* (J)-injected animals. (K) Overexpression of mHTT did not change DCP1A and AGO2 colocalization. n = 6 (3 animals/group).

(L) Venn diagram showing the number of unique and shared target genes of let-7, miR-9, and miR-128, as predicted by TargetScan. Only genes with more than 16 reads on average were included and used in the downstream miRNA target analysis. n = 3 (1 animal/ RNA sample).

(M) Cumulative fractions of $\log_2$(mHTT/wtHTT) fold changes of expressed genes (>16 reads) and the predicted targets of let-7, miR-9, and miR-128 as well as the 38 shared targets show a significant upregulation in AAV-*mHTT* compared to AAV-*wtHTT*-injected animals. n = 3 (1 animal/sample). *p < 0.05, ***p < 0.001; Wilcoxon rank-sum test with continuity correction was applied to target genes versus all genes).

(N) The top 12 most enriched Panther gene ontologies among the set of significantly upregulated ($\log_2$ fold-change > 0.1; *p < 0.05, n = 183) let-7, miR-9, and miR-128 target genes. Fold enrichment: observed number of genes/expected from background population of all expressed genes (>16 reads). Black triangles: p value, binomial distribution test. Numbers by bars indicate the number of observed genes for the given term.

All fold changes are shown as $\log_2$(mHTT/wtHTT). WB values were normalized to AAV-*wtHTT*-injected expression levels and corrected to actin values. ***p < 0.001; **p < 0.01; *p < 0.05; two-tailed two-sample unequal variance t tests. All data are shown as mean ± SEM. Scale bars represent 5 μm (D and E) and 7.5 μm (I and J). See also Figure S5 and Tables S1, S2, S4, S5, and S6.

performed in cancer cell lines found that AGO2 accumulation because of impaired autophagy results in a loss of mature miRNAs. In this study, the authors speculated that this phenomenon was due to an imbalance in the stoichiometry of the RISC complex components (Gibbings et al., 2012). When we analyzed 293T cells expressing mHTT, we found similar results, including global loss of mature miRNAs (Figures S5L and S5M). However, mature neurons do not divide, and, thus, any impairments in autophagy are likely to have different consequences than in dividing cells, which can renew their cytoplasmic content upon cell division.

We found that accumulation of AGO2 in neurons expressing mHTT is linked to accumulation of mature miRNAs. However, mHTT expression also causes a shift in AGO2 localization to SGs, resulting in global loss of miRNA activity despite the increase in mature miRNAs. It thus appears that the consequence of AGO2 accumulation is fundamentally different between neurons and dividing cells, which could be due to the inability of neurons to renew their protein composition during cell division or through the appearance of SGs in mHTT-expressing neurons.

In this study, we used an AAV-based *in vivo* mouse model. This model has several advantages for studying the transcriptional response to mHTT because it allows for an appropriate control (AAV-*wtHTT*) and results in neuron-specific expression of mHTT, limiting the effect on surrounding glial cells that otherwise may complicate the analysis. Compared to most transgenic mouse models of NDDs, it also avoids potential developmental or compensatory effects that might arise because of transgene expression in the entire organism during brain development. Our data show that alterations in AGO2 levels following mHTT expression occur at an early time point during the disease course. AGO2 and mature miRNAs are already accumulating 3 weeks following AAV-*mHTT* injection, a time point when only minor alterations in neuronal functions can be detected, as monitored by DARPP-32 levels or electrophysiological recordings. This suggests that loss of miRNA activity may be an important component of early disease phenotypes in HD. In this respect, our data are in line with a previous study that found a global accumulation of miRNAs at an early stage in a mouse model of HD, and there are also data indicating that mHTT expression impairs miRNA silencing in cell lines (Lee et al., 2011; Savas et al., 2008). In contrast, our results are inconsistent with several reports of either selective up- or downregulation of individual miRNAs or reports of a global loss of miRNAs in more severe HD mouse models or when analyzing post-mortem tissue (Kocerha et al., 2014; Maciotta et al., 2013). This discrepancy may, to some extent, be explained by differences in methodology as well as some limitations when using various mouse models and post-mortem material. Alternatively, it may also result from the fact that impairments of the miRNA machinery change as the disease progresses. When we analyzed striatal tissue 6 months after AAV-*mHTT* injection, when there was clear evidence of striatal and ventricle volume changes that was coupled with atrophy and gliosis, thus reflecting a later-stage time point, we rather find a decrease in AGO2 protein level, as measured by WB, and only detected sparse neurons displaying AGO2 accumulation (Figures S6A–S6Y). Similar, we found lower AGO2 levels from HD post-mortem striatal tissue when analyzing global protein levels using WB (Figure S6Z). These data raise the possibility that AGO2 accumulation accompanied by a loss of miRNA activity is a specific feature of early-stage impairment in neurons expressing protein aggregates and impaired autophagy.

In summary, our results suggest that changes in miRNA levels are an early feature of HD that lies downstream of alterations in autophagy. Our data provide a mechanistic link between protein aggregation and post-transcriptional gene regulation, two seemingly unrelated phenomena. Our data also provide further support for developing autophagy-activating therapeutic approaches for HD and other NDDs because they suggest that activation of autophagy will not only clear toxic protein aggregates but also directly restore dysfunctional post-transcriptional gene regulation.

EXPERIMENTAL PROCEDURES

Detailed experimental procedures can be found in the Supplemental Experimental Procedures.

Viral Vectors

To overexpress wtHTT and mHTT, we used previously described third-generation self-inactivating lentiviral vectors encoding the first 171 amino acids of the human huntingtin gene with 18 or 66 CAG repeats under the control of a mouse phosphoglycerate kinase 1 promoter (PGK) (de Almeida et al., 2002).

Animal Surgery

All animal-related procedures were approved and conducted in accordance with the Committee for Use of Laboratory Animals at Lund University. All mice were adult C57BL/6 females 9 to 10 weeks old at the time of surgery. All stereotactic injections into the striatum were performed as described before with minor changes (Petri et al., 2017). Injections were unilateral on the right side of the brain with a total of 1 μl of injected virus. The injection coordinates were as follows: anterior/posterior (AP): +0.9 mm; medial/lateral (ML): +/−1.8 mm; dorsal/ventral (DV) (from the dura): −2.7 mm.

Human Tissue

Post-mortem human brain tissue was obtained from the Cambridge Brain Bank (Cambridge, UK) and used under local ethics approval (REC 01/177).

Small RNA-Seq

cDNA libraries of small RNA-seq samples were prepared using the New England Biolabs Small RNA Library Prep Kit for small RNA-seq at the Clinical Microarray Core (University of California, Los Angeles [UCLA], CA, USA). Illumina high-throughput sequencing was applied to the samples (total number of reads: *in vivo*, 228,894,902; *in vitro*, 71,800,132).

RNA-Seq

cDNA libraries of the *in vitro* mRNA samples were prepared using the KAPA Stranded mRNA-Seq Kit from KAPAbiosystems at the Clinical Microarray Core (UCLA, CA, USA). *In vivo* cDNA libraries were prepared using the Illumina Strand-Specific TruSeq RNA Library Kit using poly(A) selection and sent for sequencing to SciLifeLab. Illumina high-throughput sequencing was applied to all the samples (total read number: *in vitro*, 180,491,336; *in vivo*, 356,983,073).

Statistical Analysis

Two-tailed, two-sample unequal variance t tests were used to analyze means in most cases. One-way ANOVA or nonparametric Kruskal-Wallis test was used in Figures 1B, S1B–S1D, S1M, and S1N with Figures S1Q and S1S depending on normal distribution defined by D'Agostino-Pearson omnibus normality test. The criterion for significance for all analyses was $p < 0.05$. All data are shown as mean ± SEM.

DATA AND SOFTWARE AVAILABILITY

The accession number for the RNA-seq and small RNA-seq data reported in this paper is GEO: GSE78928.

SUPPLEMENTAL INFORMATION

Supplemental Information includes Supplemental Experimental Procedures, six figures, and six tables and can be found with this article online at https://doi.org/10.1016/j.celrep.2018.07.017.

ACKNOWLEDGMENTS

We are grateful to all members of the Jakobsson lab as well as Bengt Mattsson and Janelle Drouin-Ouellet for stimulating discussions and useful comments on the manuscript. We also thank U. Jarl, J. Johansson, M. Persson Vejgården, I. Nilsson, E. Ling, M. Sparrenius, U. Samuelsson, A. Josefsson, and A. Hammarberg for technical assistance. We thank the Cambridge Brain Bank for the post-mortem tissue and the support it receives from the NIHR award of a Biomedical Research Centre to Addenbrooke's Hospital and the University of Cambridge. This work was supported by grants from the Swedish Research Council (K2014-62X-22527-01-3 and K2014-62X-20404-08-5), the Swedish Foundation for Strategic Research (FFL12-0074), the Swedish Brain Foundation (FO2014-0106), the Swedish Excellence Project Basal Ganglia Disorders Linnaeus Consortium (Bagadilico), and the Swedish Government Initiative for Strategic Research Areas (MultiPark and StemTherapy).

AUTHOR CONTRIBUTIONS

K.P., R.P., S.M., P.L.B., R.V., D.R.O., I.S.-A., B.A.H., M.M.-B., S.H.L., Å.P., N.D., S.S.H., M.P., R.A.B., and J.J. designed and performed the research and analyzed data. R.P., P.L.B., and M.M.-B. performed the bioinformatics analysis. K.P. and J.J. designed and coordinated the project and analyzed data. K.P. and J.J. wrote the paper, and all authors reviewed the manuscript.

DECLARATION OF INTERESTS

The authors declare no competing interests.

Received: November 3, 2017
Revised: April 19, 2018
Accepted: July 4, 2018
Published: August 7, 2018

REFERENCES

Agarwal, V., Bell, G.W., Nam, J.W., and Bartel, D.P. (2015). Predicting effective microRNA target sites in mammalian mRNAs. eLife *4*.

Anderson, P., and Kedersha, N. (2006). RNA granules. J. Cell Biol. *172*, 803–808.

Bossé, G.D., and Simard, M.J. (2010). A new twist in the microRNA pathway: Not Dicer but Argonaute is required for a microRNA production. Cell Res. *20*, 735–737.

Cheng, S., Zhang, C., Xu, C., Wang, L., Zou, X., and Chen, G. (2014). Age-dependent neuron loss is associated with impaired adult neurogenesis in forebrain neuron-specific Dicer conditional knockout mice. Int. J. Biochem. Cell Biol. *57*, 186–196.

Cortes, C.J., and La Spada, A.R. (2014). The many faces of autophagy dysfunction in Huntington's disease: from mechanism to therapy. Drug Discov. Today *19*, 963–971.

de Almeida, L.P., Ross, C.A., Zala, D., Aebischer, P., and Déglon, N. (2002). Lentiviral-mediated delivery of mutant huntingtin in the striatum of rats induces a selective neuropathology modulated by polyglutamine repeat size, huntingtin expression levels, and protein length. J. Neurosci. *22*, 3473–3483.

Diederichs, S., and Haber, D.A. (2007). Dual role for argonautes in microRNA processing and posttranscriptional regulation of microRNA expression. Cell *131*, 1097–1108.

DiFiglia, M., Sapp, E., Chase, K.O., Davies, S.W., Bates, G.P., Vonsattel, J.P., and Aronin, N. (1997). Aggregation of huntingtin in neuronal intranuclear inclusions and dystrophic neurites in brain. Science *277*, 1990–1993.

Füllgrabe, J., Klionsky, D.J., and Joseph, B. (2014). The return of the nucleus: transcriptional and epigenetic control of autophagy. Nat. Rev. Mol. Cell Biol. *15*, 65–74.

Gibbings, D., Mostowy, S., Jay, F., Schwab, Y., Cossart, P., and Voinnet, O. (2012). Selective autophagy degrades DICER and AGO2 and regulates miRNA activity. Nat. Cell Biol. *14*, 1314–1321.

Gray, M., Shirasaki, D.I., Cepeda, C., André, V.M., Wilburn, B., Lu, X.H., Tao, J., Yamazaki, I., Li, S.H., Sun, Y.E., et al. (2008). Full-length human mutant huntingtin with a stable polyglutamine repeat can elicit progressive and selective neuropathogenesis in BACHD mice. J. Neurosci. *28*, 6182–6195.

He, M., Liu, Y., Wang, X., Zhang, M.Q., Hannon, G.J., and Huang, Z.J. (2012). Cell-type-based analysis of microRNA profiles in the mouse brain. Neuron *73*, 35–48.

Kocerha, J., Xu, Y., Prucha, M.S., Zhao, D., and Chan, A.W. (2014). microRNA-128a dysregulation in transgenic Huntington's disease monkeys. Mol. Brain *7*, 46.

Lee, S.T., Chu, K., Im, W.S., Yoon, H.J., Im, J.Y., Park, J.E., Park, K.H., Jung, K.H., Lee, S.K., Kim, M., and Roh, J.K. (2011). Altered microRNA regulation in Huntington's disease models. Exp. Neurol. *227*, 172–179.

Leung, A.K., and Sharp, P.A. (2013). Quantifying Argonaute proteins in and out of GW/P-bodies: implications in microRNA activities. Adv. Exp. Med. Biol. *768*, 165–182.

Maciotta, S., Meregalli, M., and Torrente, Y. (2013). The involvement of microRNAs in neurodegenerative diseases. Front. Cell. Neurosci. *7*, 265.

Martin, D.D., Ladha, S., Ehrnhoefer, D.E., and Hayden, M.R. (2015). Autophagy in Huntington disease and huntingtin in autophagy. Trends Neurosci. *38*, 26–35.

Pang, X., Hogan, E.M., Casserly, A., Gao, G., Gardner, P.D., and Tapper, A.R. (2014). Dicer expression is essential for adult midbrain dopaminergic neuron maintenance and survival. Mol. Cell. Neurosci. *58*, 22–28.

Petri, R., Malmevik, J., Fasching, L., Åkerblom, M., and Jakobsson, J. (2014). miRNAs in brain development. Exp. Cell Res. *321*, 84–89.

Petri, R., Pircs, K., Jönsson, M.E., Åkerblom, M., Brattås, P.L., Klussendorf, T., and Jakobsson, J. (2017). let-7 regulates radial migration of new-born neurons through positive regulation of autophagy. EMBO J. *36*, 1379–1391.

Qi, H.H., Ongusaha, P.P., Myllyharju, J., Cheng, D., Pakkanen, O., Shi, Y., Lee, S.W., Peng, J., and Shi, Y. (2008). Prolyl 4-hydroxylation regulates Argonaute 2 stability. Nature *455*, 421–424.

Savas, J.N., Makusky, A., Ottosen, S., Baillat, D., Then, F., Krainc, D., Shiekhattar, R., Markey, S.P., and Tanese, N. (2008). Huntington's disease protein contributes to RNA-mediated gene silencing through association with Argonaute and P bodies. Proc. Natl. Acad. Sci. USA *105*, 10820–10825.

Schaefer, A., O'Carroll, D., Tan, C.L., Hillman, D., Sugimori, M., Llinas, R., and Greengard, P. (2007). Cerebellar neurodegeneration in the absence of microRNAs. J. Exp. Med. *204*, 1553–1558.

Tan, C.L., Plotkin, J.L., Venø, M.T., von Schimmelmann, M., Feinberg, P., Mann, S., Handler, A., Kjems, J., Surmeier, D.J., O'Carroll, D., et al. (2013). MicroRNA-128 governs neuronal excitability and motor behavior in mice. Science *342*, 1254–1258.

Wu, C., So, J., Davis-Dusenbery, B.N., Qi, H.H., Bloch, D.B., Shi, Y., Lagna, G., and Hata, A. (2011). Hypoxia potentiates microRNA-mediated gene silencing through posttranslational modification of Argonaute2. Mol. Cell. Biol. *31*, 4760–4774.

Yamamoto, A., and Yue, Z. (2014). Autophagy and its normal and pathogenic states in the brain. Annu. Rev. Neurosci. *37*, 55–78.